A Global Design Search of a Shrouded Tidal Current Turbine by Meta-model Assisted Genetic Algorithms

Benson Oyunge Mwangi, Ngome Adam Mwero, Reiko Yamada, Patxi Garcia Novo, Yusaku Kyozuka, Daisaku Sakaguchi

Abstract-This study was conducted to investigate the effect of geometry on the performance of a shrouded tidal turbine. When the hub radius and taper change, with a fixed shroud radius, the inlet area changes from the inlet to the turbine, and according to the continuity equation, the inlet axial velocity will also change. This inlet velocity, U1 influences the output torque by a factor of U₁³ for the power coefficient especially for such a case with constant turbine rotation speed as this. In this study, a global search optimization system was used to search for the optimal geometry. 13 impeller design parameters and 5 shroud casing design parameters were considered for optimization. To reduce the simulation cost, an artificial neural network (ANN) was applied as the meta-model of the RANS solver. Multi-objectives of a power coefficient at different tip speed ratios were applied to provide a function of the wide operating range of the turbine. The proposed optimized turbine design exhibits a high output shaft power at low tipspeed ratios. Increasing the hub radius caused a strong velocity gradient at the turbine inlet. Hence, achieving smooth blade loading from the hub to the shroud for the baseline is difficult. However, this inlet axial velocity distortion decreased in the optimal geometry, attaining smooth blade loading from the hub to the shroud. This results in higher torque output and, hence, higher power coefficient, CPO values in the optimal geometry. From the sensitivity analysis of the design parameters with C_{P0}, there is a good global correlation between the axial velocity upstream of the turbine and the C_{P0} . A strong circumferential velocity occurs in the optimal diffuser, causing a centrifugal force at the shroud tip, suppressing the diffuser's flow separation. This improves the pressure recovery and performance of the optimal design.

Keywords—Multi-objective optimization, Genetic algorithm, Artificial neural network, Tidal current turbine, Sensitivity analysis.

Part of a special issue for AWTEC 2024. Manuscript submitted 3 March 2024; Revised 11 March 2025; Accepted 1 June 2025. Published 20 October 2025.

This is an open access article distributed under the terms of the Creative Commons Attribution 4.0 International license. CC BY https://creativecommons.org/licenses/by/4.0/. Unrestricted use (including commercial), distribution and reproduction is permitted provided that credit is given to the original author(s) of the work, including a URI or hyperlink to the work, this public license and a copy right notice. This article has been subject to a single-blind peer review by a minimum of two reviewers.

Digital Object Identifier: https://doi.org/10.36688/imej.8.367-377

I. Introduction

The research to improve the performance of tidal current turbines has received a lot of attention in the recent past. Their design is similar to the wind turbine design, even though it is used in the marine environment to capture kinetic energy from currents and convert it to electrical energy. For instance, Ohya and Karasudani [1] developed a new broad-ring brim at the periphery of a wind turbine. They reported an improvement in the performance of the brimmed diffuser in that the strong vortex formed behind it contributes to drawing more flow at the inlet of the turbine hence higher power coefficient values resulting from better pressure recovery in the diffuser. On the other hand, Hashem et al. [2] numerically investigated the effect of a brimmed diffuser on the performance of a small-scale wind turbine. They also noted that the brimmed diffuser increased the output power coefficient of the shrouded turbine compared to the unshrouded one for the same wind speed and similar turbine characteristics. Moreover, in their study, Weichao et al. [3] numerically and experimentally investigated the effects of the leading-edge tubercles, mimicked from the humpback whale, on the performance of a hydrofoil. They established that these tubercles could improve the lift-todrag ratio and reduce the tip vortex, hence improving the turbine's performance. Fu-wei et al. [4] optimized the blade chord length and the pitch angle distribution of a horizontal tidal turbine. They reported a power coefficient increase of 2% as well as an expanded tip speed ratio range. Also, Zhang et al. [5] conducted an optimization study on the blade profiles of a horizontal axis tidal turbine using blade element momentum (BEM) theory coupled with CFD calculation. A 4.1% improvement of the mean power coefficient and a decrease of 46.7% in its variance was achieved. Kunasekaran et al. [6] used a winglet at the tip of a turbine blade and reported a 7% increase in power coefficient, an increased pressure gradient, and a reduced tip vortex. Smirnov et. al. [7] have studied the effects of the hub end wall geometry and the rotor leading edge shape, separately, on the performance of a supersonic axial impulsive turbine. They reported that the hub end wall modification resulted in an efficiency increase of up to 2%, whereas the rotor leading edge shape modification did not provide any significant efficiency increase when compared

with the baseline. On the other hand, Akin et. al. [8] optimized the hub end wall contour of a turning midturbine frame to maximize the isentropic efficiency of a turbine low-pressure stage. They also compared the results between different optimization strategies. Findings from Fan et al. [9] demonstrate that a tidal turbine with leading edge tubercles (Bio-turbine) has higher energy conversion performance, especially at higher TSRs compared to the baseline turbine. This Bio-turbine also affects pressure distribution and flow separation behaviour on the suction side, causing an enlarged wake recovery area. Blade load fluctuations for a tidal turbine were reduced by using a winglet, hence improving its efficiency, especially at a cant angle of 45° [10].

Moreover, Mohamed et al. [11] were able to demonstrate the effect of the winglet length and cant angle on the performance of a small-scale horizontal-axis wind turbine. Similarly, Marina et al. [12] were able to show that winglets at the tip of the blade can subdue the strength of tip vortices, hence improving performance for blades with winglets compared to those without. On the other hand, Ren et al. [13] [14] investigated the effect of the winglet shape on the performance of a horizontal tidal turbine. Saravanan et al. [15] experimentally established that there is a correlation between the winglet height and curvature radius on the performance of a small horizontal wind turbine.

Even though the effect of geometry on the performance of a horizontal-axis tidal turbine has been studied by many researchers, still there is limited research on the effect of the hub radius and the taper geometry on the performance of an axial tidal turbine. Therefore, in this study, the effect of the hub radius and taper on the performance of a shrouded tidal turbine was investigated. A total of 13 design parameters for the impeller and 5 for the shroud casing were considered for the optimization. This study was based on a previous study by Nagataki et al. [16] in which 11 parameters were chosen for the impeller and 4 for the shroud casing. Also, in the previous study, the hub radius and taper were fixed. However, in the current study, these parameters were varied, and therefore, additional design parameters were needed. Moreover, all these design parameters were carefully selected to achieve the objective of this study. A global search optimization system -the Von Karman Institute of Fluid Dynamics (VKI) optimizer- was used to search for the optimal geometry. Multi-objectives of power coefficient at different tip speed ratios were applied to provide a function of the wide operating range of the turbine.

Nomenclature

0 in Fig. 1 represents the inlet boundary for the $\widehat{\text{sim}}$ nulation domain

in Fig. 1 represents the turbine blade station CFD means Computational Fluid Dynamics D_1 represents the turbine diameter T is the symbol for torque

 C_{p0} represents the power coefficient with respect to the flow condition at station 0, as shown in Fig. 1.

 λ_0 is the tip speed ratio

 ω is the angular velocity of the turbine in rad/sec

 U_0 is the flow velocity at the inlet boundary (station 0)

 ρ is the water density

 A_1 is the effective flow area at the turbine blade.

 θ is the diffuser angle

II. NUMERICAL ANALYSIS AND OPTIMIZATION METHOD

A. Numerical Method

The target turbine for this analysis was a Water Lens Turbine (WLT) of diameter, D_1 =1200mm. It was shrouded with a shroud casing of an equivalent diameter but with a tip clearance of 1% of the turbine diameter for the turbine to rotate freely. The sketch of the shrouded turbine model is shown in Fig. 1. It had 3 blades, and the blade thickness distribution was based on the NACA4616 aerofoil [16]. For the numerical simulation, the inlet boundary was set to $2.5\,D_1$ upstream of the turbine inlet, whereas the outlet boundary was set to $20D_1$ downstream of the turbine inlet.

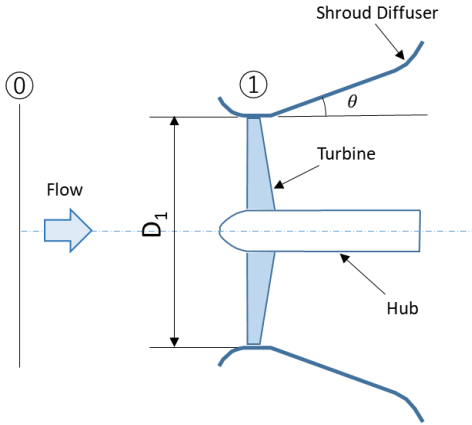


Fig. 1 Meridional section of a shrouded horizontal axis current turbine [16]

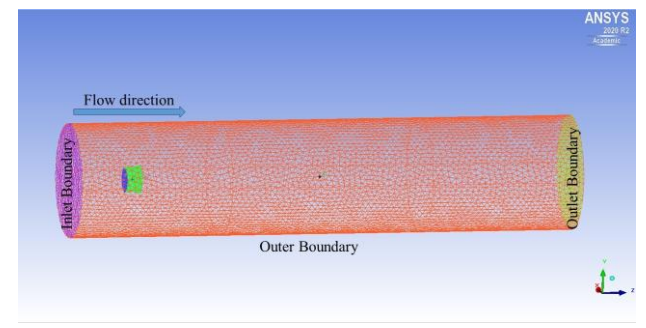


Fig. 2 Simulation domain

The outer boundary was set to 5D₁, as shown in Fig. 2 for the simulation domain. This simulation domain was arrived at after conducting several simulation domain analyses to pick the best domain in which the boundaries do not influence the flow in any way and hence the result. The numerical domain comprised a stationary domain and a rotating domain. For the stationary domain, ICEM CFD was used to generate the mesh, whereas for the rotating

The steady-state numerical simulations were conducted using a commercial Computational Fluid Dynamics (CFD) code ANSYS-CFX version 20.2. In this study, about 123,000 nodes of unstructured mesh were used in the stationary domain, whereas 150,000 nodes of structured mesh were used in the rotating domain. The Frozen Rotor Interface connected the domains, and the working fluid was water. The turbulence model that was used is the Shear Stress Turbulence (SST) model. The study was conducted at design and off-design conditions. For the design condition, the axial inlet velocity at the inlet boundary was 3 m/s, whereas this velocity was 1.5 m/s for the off-design condition. The rotational speed of the turbine was kept constant at 115 rpm. A power coefficient, CP0 curve was plotted for the optimal and baseline geometries by varying the tip speed ratio as shown in Eq. (1) to understand the improvement in performance between the two designs. This power coefficient C_{P0} is the output shaft power that has been normalized by using a reference effective flow area, A₁at the turbine blade inlet using Eq. (2). Where T is the output torque, ω is the angular velocity of the turbine, ρ is the water density, U₀ is the axial inlet velocity at the inlet boundary and D₁ is the turbine diameter. The effective flow area, A₁, was calculated using the difference between the area of the turbine and the cross-sectional area of the hub. From Fig. 1, station 0 is at the inlet boundary $(2.5D_1 \text{ upstream of the turbine})$, and station 1 is at the turbine station. Since this is a shrouded turbine, the flow velocity at station 0, U₀, is not the same as the velocity at station 1, U₁, because the flow is accelerating due to the effect of the shroud. Therefore, the power coefficient is calculated using U₀ because it is an important parameter when estimating the output power and the flow condition of the tidal flow. This is why the power coefficient has been abbreviated by C_{P0} in this study.

$$\lambda_0 = \frac{D_1 \cdot \omega}{2 \cdot U_0} \tag{1}$$

$$C_{P0} = \frac{T.\omega}{0.5.\rho. A_1.U_0^3}$$
 (2)

The unique point of this study was varying the hub radius and taper geometry. The hub radius was varied between 0.1 m and 0.3 m, and the hub taper was also varied by setting limits for its respective control points. This was done to investigate the effect of geometry on the turbine's performance. Given that the shroud radius does not change, as the hub radius and taper change, the inlet area changes from the inlet to the turbine, and according to the continuity equation, the axial velocity will also change. It is worth noting that this study is for a fixed speed turbine (115 rpm). Hence, for this case, it can be seen from Eq. (2) that the inlet flow velocity, U_1 , influences the

output torque by a factor of U₁³ for the power coefficient. Therefore, it is expected that the torque values will increase when the inlet velocity increases. This axial velocity component was compared between the baseline and the optimal geometry to understand how it influences the turbine blade loading from the hub to the shroud and how this further influences the output shaft torque between the two designs. During the optimization process, the hub radius was varied, and this caused a respective variation in the blade geometry. For instance, the blade span and the chord length were varied as a result because the blade and the shroud were optimized simultaneously. This also changes the effective area of flow between the hub and the shroud casing. The torque was calculated from the force obtained from the product of the integrated value of pressure distribution around the blade and the area of the blade. The location of calculation for torque was selected on the blade whose axis of rotation was the zaxis. Then, the obtained torque values were used to calculate the power coefficient using Eq. 2.

B. Optimization Method

The optimization system used in the current study was developed by the Von Karman Institute for Fluid and it has been applied to various turbomachinery studies. This design and optimization study using GA and ANN tools is applicable for other tidal turbines as well, including the vertical axis tidal turbines. It can also be used in other systems, such as wind turbines and other turbomachines in general. For example, Tun et al. [19] and Sakaguchi et al. [20], have conducted multiobjective optimization on centrifugal compressors and centrifugal blowers, respectively, using this method. Generally, this optimization process is shown in Fig. 3. The vertical flow on the left side of the figure represents the traditional CFD design procedure in which theoretical consideration and experimental experience play a vital role. The right side shows the two levels involved in the optimization process: Level 1 and Level 2. The upper right box (Level 1) represents the optimization loop comprising a differential evolution algorithm (DE) and a meta-model based on an Artificial Neural Network (ANN). The ANN has been used to replace the computationally expensive CFD simulations in the optimization loop (Level 1). It provides less accurate but very fast performance predictions, and this is very useful in evaluating a large number of geometries by the DE algorithm during the search for the optimum design. In the process of searching for the optimum geometry, it is necessary to train the metamodel, and for this reason, a database is required from past reliable numerical data. Therefore, the database for the current study was initialized by way of a Design of Experiment (DOE) comprising 128 designs. This database was generated before the optimization loop (Level 1) was started. The optimization loop (Level 1) was invoked after building the database and training the meta-model (ANN). Then, DE started the prediction of the optimal geometries.

Since the ANN is less accurate than the traditional CFD, it requires validation, which is performed by the feedback loop (Level 2). In this validation, the output optimal geometries from the ANN prediction are confirmed by the more computationally accurate but expensive CFD calculations to verify the accuracy of the meta-model (Level 2). After validation, the results are added to the database, and a new optimization loop is started after a new training of the meta-model based on the enlarged database.

C. Objective Function and Design Parameters

The maximum speed of the tidal current at the experimental site of interest, i.e., GOTO Island in Japan, is 3 m/s, which corresponds to a design tip speed ratio (TSR) of $\lambda_0=2.0$. Whereas, the medium speed of the tidal current is 1.5 m/s, corresponding to an off-design TSR of $\lambda_0=4.0$ [17]. An ideal speed of the tidal flow changes in a sinusoidal manner with a period of almost every 6 hours, as shown in Fig. 4. The main optimization objective in this study is to maximize the power coefficient at design and off-design TSRs.

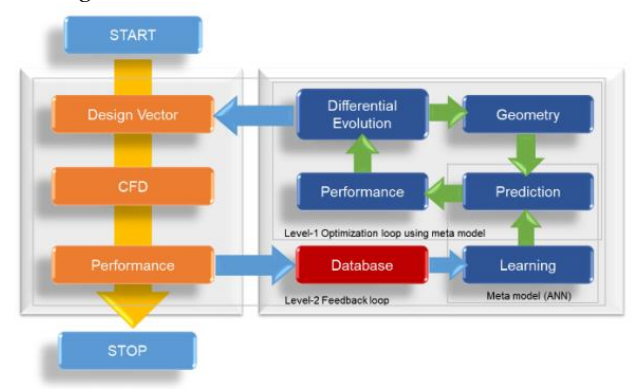


Fig. 3 General Layout of the VKI Optimization System [18]

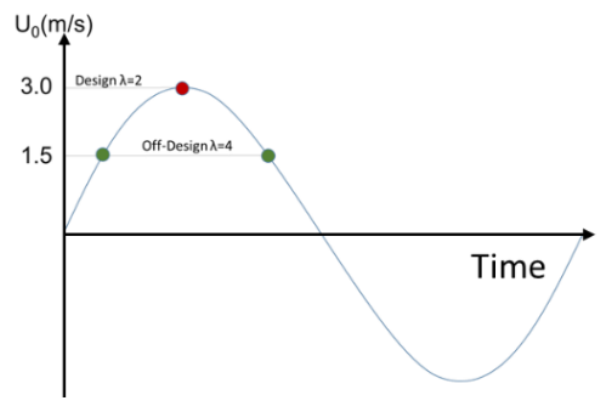


Fig. 4 The sinusoidal nature of tidal current velocity [18]

During the optimization process, each design parameter was set to a lower and upper limit, as shown in **Error! Reference source not found.**. For the turbine blade, t he blade angle and chord length change from the hub to the shroud, and a point of inflection is introduced to have a three-dimensional (3-D) shape of the turbine.

Table 1 Design parameters for optimization of the Water Lens ${\it Turbine}$

opt #	Impeller Hub		Min	Max
opt- 1	Blade angle at LE (Hub side) deg.		5	15
opt- 2	Delta_Beta_12	deg.	5	15
opt- 3	Delta_HubBeta_23	deg.	0	10
opt-	Meridional position of blade TE (Hub side)	m	0.08 0.15	
opt- 5	Nacelle cylinder radius	m	0.1 0.3	
opt-	Hub taper radius	m	-0.15	-0.10
	Impeller Mid 1			
opt-	Span position of control point	-	0.1	0.5
opt-	Blade angle at LE	deg.	0	7.5
opt- 9	Blade angle at TE	deg.	-20	0
	Impeller Shroud			
opt- 10	Blade angle at LE (Shroud side)	deg.	55	62
opt- 11	Delta_ShroudBeta_12	deg.	0	15
opt- 12	Delta_ShroudBeta_23	deg.	0	5
opt- 13	Meridional position of blade TE (Shroud side)	m	0.03	0.05
	Shroud Casing			
opt- 14	Shroud inlet length	m	-0.30	-0.25
opt- 15	Shroud inlet radius	m	0.68	0.63
opt- 16	Shroud outlet length1	m	0.40	0.74
opt- 17	Shroud outlet radius1	m	0.70	0.85
opt- 18	Shroud outlet radius2	m	0.17	0.2

A couple of control points were used on the shroud and hub to achieve the required geometry. As shown in Fig. 5, four control points (Opt-14, 15, 16, and 17) for the shroud casing are adopted to achieve the conical diffuser length and diameter. Additionally, parameter Opt-18 is used to achieve a smooth extension of the diffuser exit. Two control points (Opt-5 and 6) are used to achieve the desired hub radius and taper geometry, respectively. Since this device is symmetrical along the z-axis, only its half is shown in Fig. 5. The design parameters in Error! Reference source not found. have been described in detail in the Appendix I.

In this study, the baseline was an existing model that was designed previously by Nagataki et al. [16]. But to fit

III. RESULTS AND DISCUSSION

The optimization process involved a correlation of two objective functions which are; the design C_{P0} and the off-design C_{P0} . The obtained result is shown in Fig. 6. The horizontal axis represents the power coefficient C_{P0} at the design TSR, $\lambda_0=2.0$, and the vertical axis represents the power coefficient C_{P0} at the off-design TSR, $\lambda_0=4.0$. In this analysis, the objective functions were multiplied by 1; therefore, the optimal geometry approaches the bottom left corner.

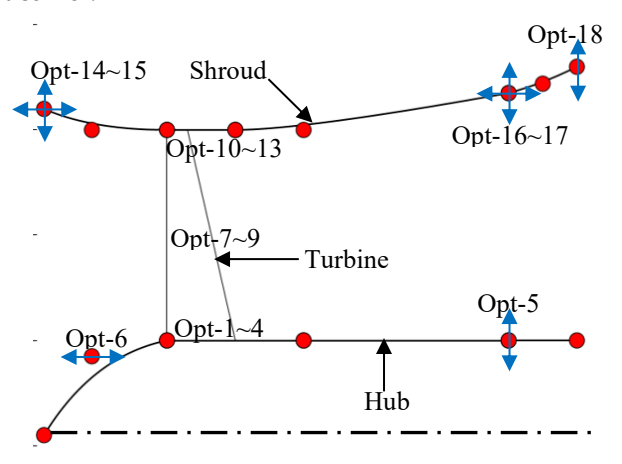


Fig. 5 Control points of design variables for optimization

From Fig. 6, the grey circles show individuals that were obtained during the DOE process at the point of initial learning by the ANN, whereas the red ones show those that have met the design constraints set during the optimization process. A total of about 220 individuals were considered during the optimization process in the Level 2 loop, as shown in Fig. 3. As observed in Fig. 6, a hyperbolic shape forms at the front end of the individuals. This is known as the Pareto front and indicates that to pick the optimal geometry, we need to trade-off between the two objective functions and select the individual that shows a good balance between them. Therefore, improving both of them in the same turbine configuration is difficult. Five individuals were picked from the Pareto front for analysis to understand how the power coefficient varies among them.

The optimal individual was chosen from the Pareto front, considering the red circle, which fulfilled the design constraints. In this case, the individual indicated by the green circle was chosen as optimal since it shows a good balance for both objective functions. The baseline is shown by a yellow circle. The 3-dimensional shapes of the baseline and the optimal geometry are shown in Fig. 7. The figure shows that there is a significant difference between the optimal geometry and the baseline. Of great importance to this study is the hub radius and taper geometry. The optimal design has a smaller hub radius

and taper compared to the baseline. Because of this, the inlet area is smaller in the baseline than in the optimal design. This also resulted in a larger blade length (span) in the optimal design.

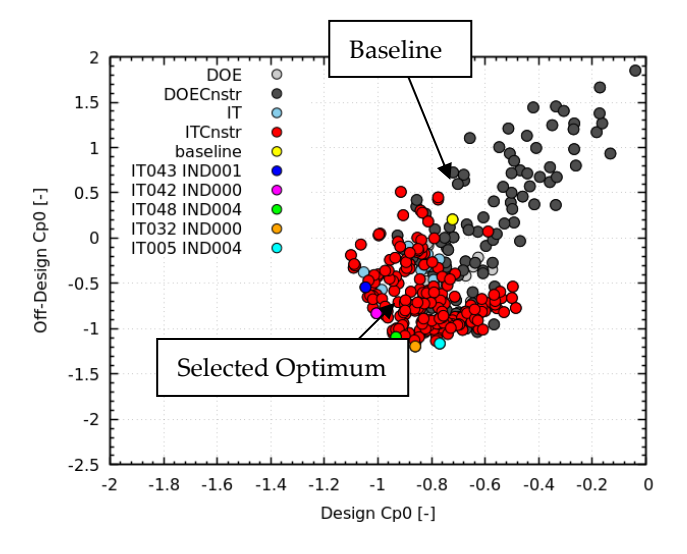


Fig. 6 Optimization results in two objective functions space.

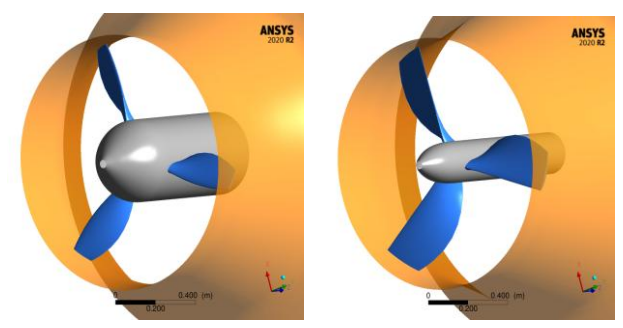


Fig. 7 Left: Baseline, and right: Optimal geometry

It is expected that when the hub radius and taper change, with a fixed shroud radius, the inlet area changes from the inlet to the turbine, and according to the continuity equation, the axial velocity will also change. This inlet flow velocity, U₁ influences the output torque by a factor of U₁³ for the power coefficient, especially for a case like this with constant turbine rotation speed. The baseline had a higher value of axial velocity into the turbine compared to the optimal geometries, as shown in From this study, it was noted that the larger hub radius and taper in the baseline caused a strong velocity gradient at the turbine inlet, as shown in Fig. 8 (a) and (b) for design and offdesign conditions, respectively. In these figures, the horizontal axis shows the axial velocity in m/s, whereas the vertical axis shows the turbine radius in meters. These inlet flow velocity values were taken at a turbo-surface at the leading edge of the turbine blade from the hub to the shroud. With this strong velocity gradient, it was difficult to achieve a smooth blade loading from the hub to the shroud at the baseline.

Table 2It was expected that higher axial velocity at the inlet of the turbine could cause a higher power coefficient.

Contrary to this, it was observed that the optimal geometry, with a smaller hub radius and taper, had the best performance characteristics compared to the baseline, with a larger hub radius and taper. The question is: Why does the smaller hub radius (optimal) result in higher C_{P0} values compared to the larger hub radius (baseline)? From this study, it was noted that the larger hub radius and taper in the baseline caused a strong velocity gradient at the turbine inlet, as shown in Fig. 8 (a) and (b) for design and off-design conditions, respectively. In these figures, the horizontal axis shows the axial velocity in m/s, whereas the vertical axis shows the turbine radius in meters. These inlet flow velocity values were taken at a turbo-surface at the leading edge of the turbine blade from the hub to the shroud. With this strong velocity gradient, it was difficult to achieve a smooth blade loading from the hub to the shroud at the baseline.

TABLE 2 INLET VELOCITY INTO THE TURBINE FOR BASELINE AND OPTIMAL DESIGNS

	Hub Radius	Axial Av. Vel [m/s] (Design)	Axial Av. Vel [m/s] (Off-design)
Baseline	0.2	4.60	2.38
IT043_IND001	0.1	4.19	2.30
IT042_IND000	0.1	3.97	2.29
IT048_IND004	0.1	3.56	2.16
IT032_IND000	0.1	3.45	2.21
IT005_IND004	0.1	3.47	2.31

However, this inlet axial velocity distortion decreased in the optimal design, attaining a smooth blade loading from the hub to the shroud. This resulted in higher output torque hence higher C_{P0} values in the optimal geometry.

Also, the performance characteristics for the individuals on the Pareto front and the baseline were analyzed and are shown in Table 3. In this table, T represents the torque in Nm and C_{P0} is the power coefficient using the velocity at the inlet boundary. From this table, it can be seen that all the geometries at the Pareto front have higher output torque values and, hence, higher power coefficient values compared to the baseline. It is also worth noting that for these geometries, the hub radius is 0.1 m (a smaller hub radius than the baseline). This interesting phenomenon is very useful in explaining the higher power coefficient value in optimal design compared to the baseline.

Regarding the diffuser angle, it can be seen that it reduces from the baseline value to a lower value in the optimal design. It is expected that larger diffuser angles will result in higher power coefficients because of better pressure recovery in the diffuser at larger angles. However, in this case, the observation was different. Since the optimal design had a smaller diffuser angle than the baseline, it was concluded that the higher power coefficient from the optimal geometry emanated from other parameters, which are its longer blade span and

diffuser length compared to the baseline. To further understand why the optimal geometry has higher power coefficient values compared to the baseline, their internal flows at design and off-design conditions are compared alongside the other performance characteristics.

TABLE 3 PERFORMANCE CHARACTERISTICS FOR OPTIMAL AND BASELINE GEOMETRIES

	Hub			Diffuser	Off-	Off-	
	Radius	Design	Design	Angle	Design	Design	Av.
	[m]	T (Nm)	_Cp0	(deg)	T (Nm)	_Cp0	Cp0
Baseline	0.2	832.22	0.72	21.12	-29.76	-0.21	0.26
IT043_IND001	0.1	1319.4	1.05	14.52	85.27	0.54	0.80
IT042_IND000	0.1	1267.9	1.01	12.44	130.7	0.83	0.92
IT048_IND004	0.1	1175.10	0.93	15.36	171.8	1.09	1.01
IT032_IND000	0.1	1085.50	0.86	19.42	188.1	1.19	1.03
IT005_IND004	0.1	970.27	0.77	21.47	183.2	1.16	0.97

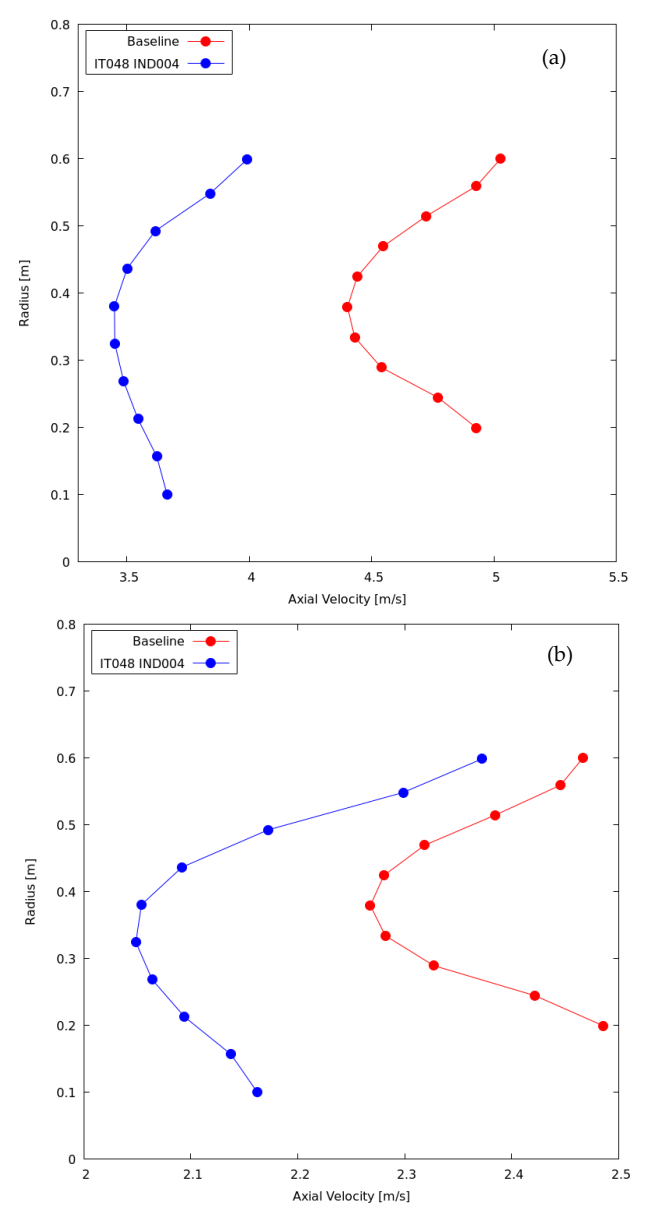
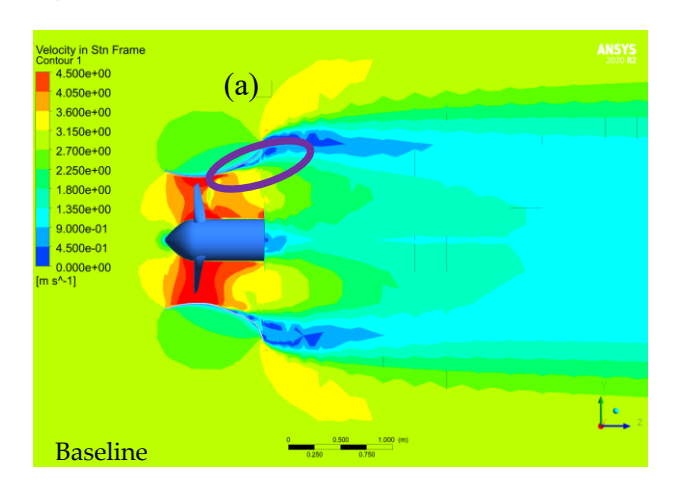


Fig. 8 Axial velocity at the turbine inlet (a) Design speed (b) Offdesign speed

The internal flow velocity results for the baseline and the optimal geometry at design and off-design conditions are shown in Fig. 9 and Fig. 10, respectively. From these

figures, it can be seen that the flow is decelerated better in the optimal diffuser (IT048_IND004) compared to the baseline. Flow separation in the diffuser can also be seen in the baseline (shown by the purple ovals on the figures). In contrast, the flow is attached well to the shroud in the optimal geometry for both design and off-design conditions. Higher flow deceleration in the diffuser results in a better pressure recovery in the optimal geometry, which in turn results in higher output torque. Because of the best combination of the diffuser and blade design of the optimal geometry, the centrifugal force that results in its diffuser is stronger compared to the one in the baseline. This centrifugal force causes better flow attachment unto the shroud and hence no flow separation for the optimal design.



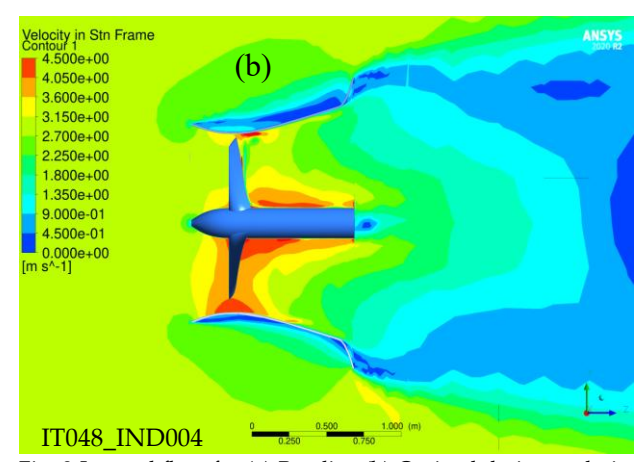
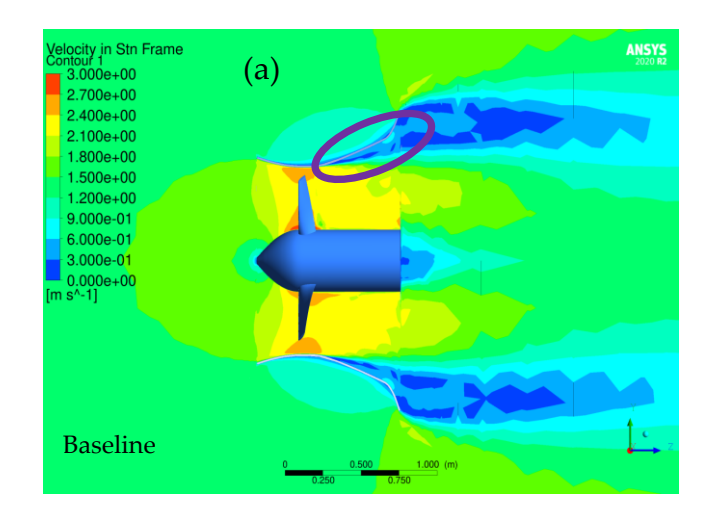


Fig. 9 Internal flow for (a) Baseline (b) Optimal design at design condition

This can be confirmed from the absolute circumferential velocity values taken at a turbo-surface just downstream of the blade trailing edge for both the baseline and the optimal design as shown in Fig. 11 (a) and (b) at design and off-design conditions, respectively. In these figures, the horizontal axis represents the absolute circumferential velocity in m/s while the vertical axis shows the turbine radius in meters. For the design condition, the values are below zero for both the baseline and optimal design, but the optimal has even lower values than the baseline, which means it has better performance than the baseline in terms of flow separation in the diffuser. For off-design condition,

the baseline values are slightly positive from the hub to the shroud, meaning that it suffers higher flow separation, which becomes pronounced at the hub side. The axial velocities at the isosurfaces were analyzed for both the baseline and the optimal design to understand the extent of flow separation occurrence in each design. From Fig. 12, it can be seen that the amount of flow separation in the diffuser was higher in the baseline. In contrast, the flow separation is minimal in the optimal design and occurs towards the exit region. This also explains why the optimal design has higher pressure recovery in the diffuser and, hence, a higher power coefficient than the baseline.

To understand the performance improvement of the optimal design, the two designs (baseline and optimal), were subjected to similar flow conditions, and their power coefficient curves were plotted and compared as shown in Fig. 13.



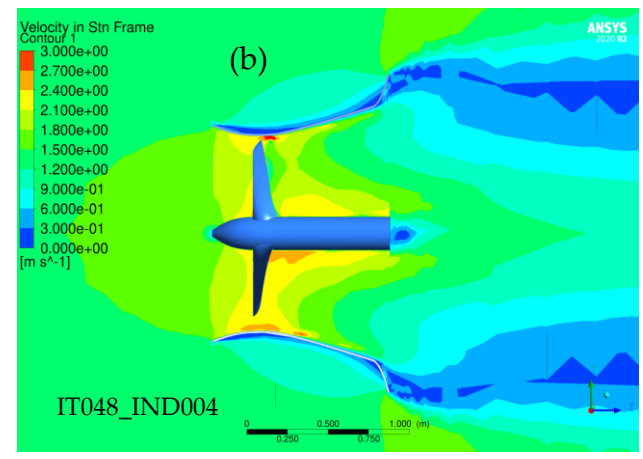


Fig. 10 Internal flow for (a) Baseline (b) Optimal design at offdesign condition

The vertical axis represents the power coefficient, whereas the horizontal axis represents the TSR. The inlet flow velocity was varied from 1 m/s to 11 m/s (TSR changed from 0.66 to 4.82). The vertical green dashed line and orange line show the design and off-design conditions, respectively. From this figure, it can be seen that the optimal design has higher C_{P0} values for all TSR values. The optimal design's power coefficient keeps increasing slightly after the design speed (λ =2.0), whereas

the one for the baseline plunges after this condition and reaches negative values at higher TSRs. This implies that at higher TSR values (lower inlet velocities), the baseline produces lower output torque, hence lower C_{P0} values, whereas the optimal design performs well in all TSR values. This is attributed to the flow separation that occurs at the blade root and the shroud side within the diffuser for the baseline, as shown in Fig. 12(a). It results in lower pressure recovery in the baseline diffuser, which in turn results in lower torque values, as seen in Table 3.

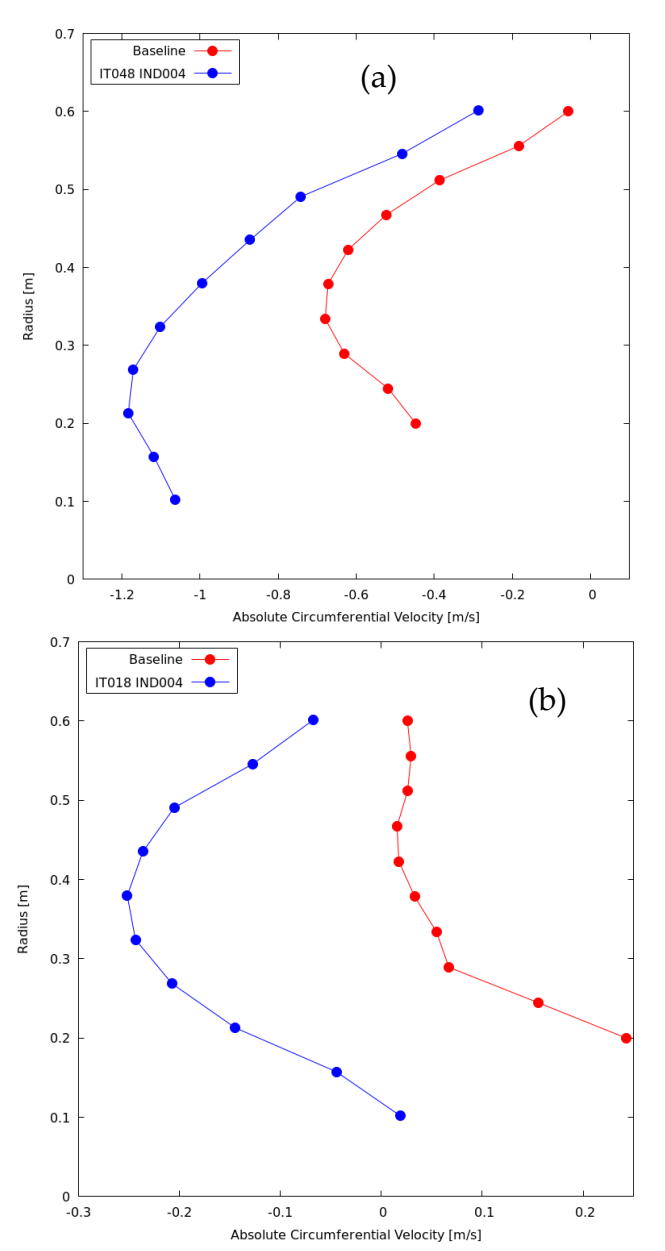
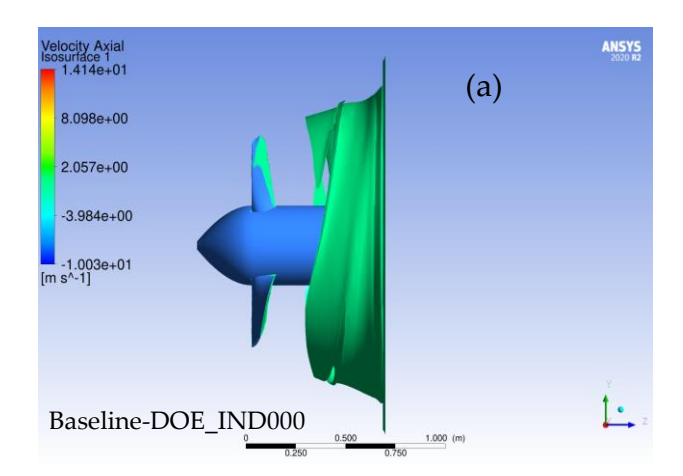


Fig. 11 Absolute Circumferential velocity for Baseline and Optimal design at (a) design and (b) off-design condition

During this optimization process, several geometries were analyzed to understand which design parameters were more sensitive to the objective functions (design and off-design power coefficients).



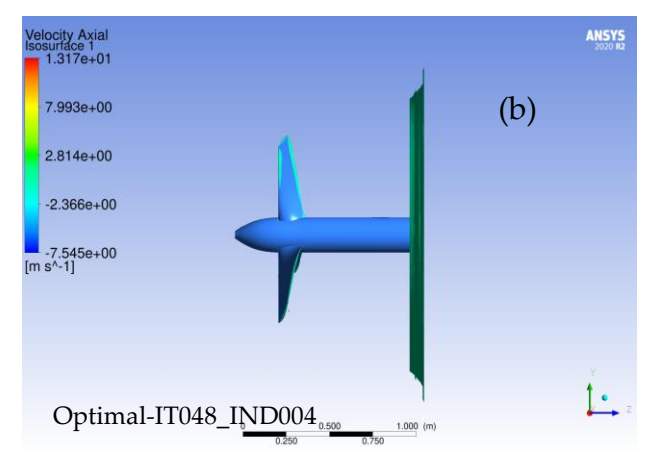


Fig. 12 Axial velocity contour for (a) Baseline and (b) Optimal design at an Isosurface

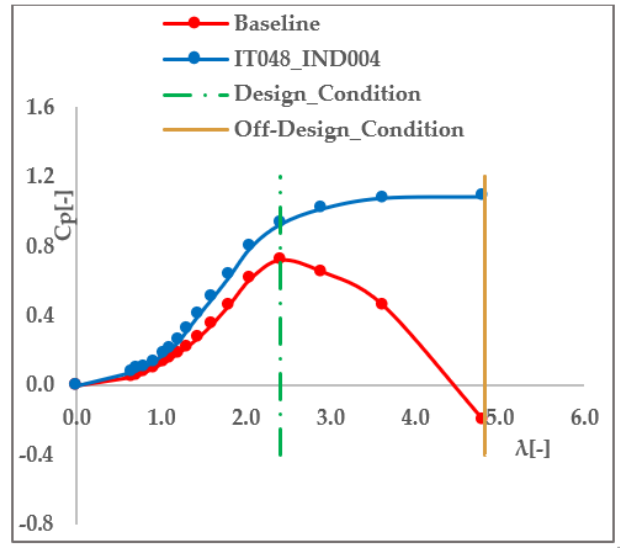


Fig. 13 Power coefficient curves for Baseline and Optimal design

From Fig. 14, it is evident that when the diffuser angle increases from the optimal value of 15 degrees to 22 degrees, the design C_{P0} worsens (green, orange, and lightblue circles), whereas the off-design C_{P0} increases. However, below 15 degrees, there is no effect on the design C_{P0} and off-design C_{P0} because the individuals (green, purple, and blue circles) are condensed together for the design condition, whereas there is no defined trend for the

off-design condition. Therefore, only higher diffuser angles affect the design and off-design C_{P0} .

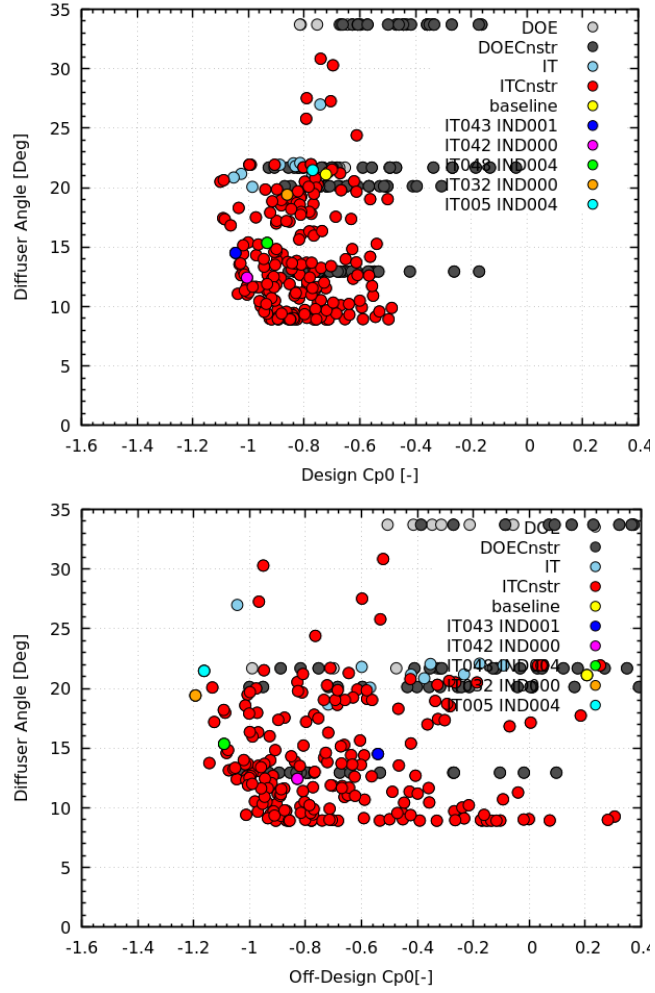


Fig. 14 Sensitivity analysis for Diffuser angle with design and off-design C_{P0}

The relationship between the axial velocity into the turbine and the power coefficient was also analyzed and plotted as shown in Fig. 15. From these figures, it can be seen that there is a good global correlation between the axial velocity and the power coefficient. They agree well with the theory that higher power coefficient values can be achieved by increasing the inlet velocity into the turbine. This is very clear from the design condition result. However, from the off-design condition, the result is a little bit scattered. Still, there is a clear limit at the bottom of the points showing a trend suggesting higher power coefficients at higher inlet velocities. Looking at the individuals picked from the Pareto front, it is evident that the optimizer picked lower axial velocity even though some individuals have higher power coefficients. This is explained by the fact that the optimal geometry had the best combination of blade and shroud design compared to the rest. Therefore, it was able to efficiently convert the kinetic energy in the lower velocity flow into the turbine (when compared to that of the baseline) to achieve the highest output torque and power coefficient.

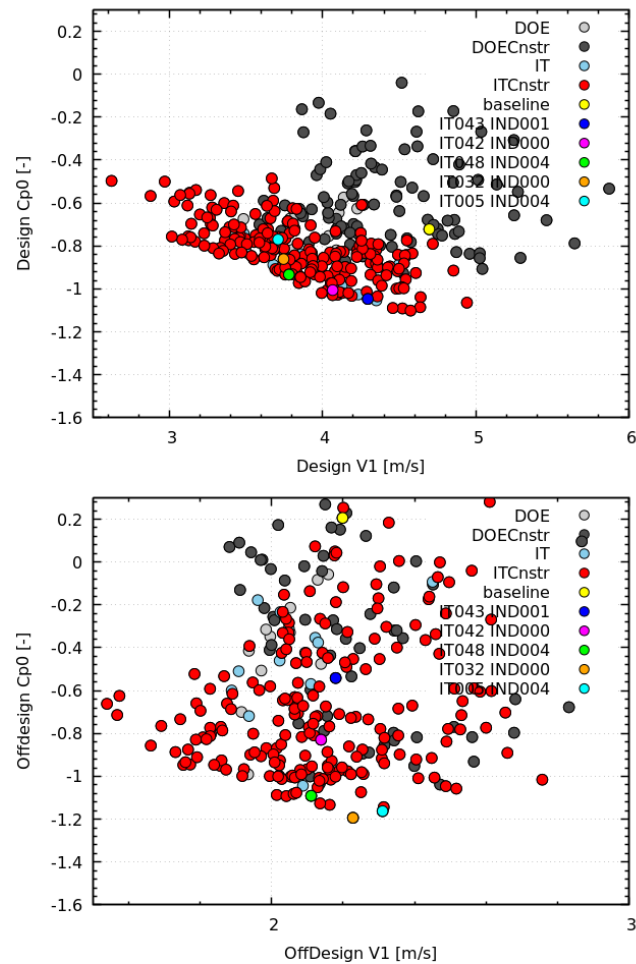


Fig. 15 Sensitivity analysis for axial velocity with design and off-design C_{P0}

Other sensitivity studies that were carried out include the relationship between the hub radius and power coefficient and between the diffuser length and the power coefficient. Their results were scattered on their plots; hence, no strong correlation was established between them and the power coefficient. For example, when the hub radius was increased, the inlet velocity became skewed, and hence, it was difficult to correlate with the power coefficient. These parameters did not contribute much to the improvement of the power coefficient.

IV. CONCLUSIONS

The effect of geometry on the performance of a shrouded horizontal-axis tidal current turbine (Water Lens turbine) was successfully investigated. From the findings, the hub radius and taper geometry influenced the effective inflow area and, hence, the flow velocity into the turbine. A larger hub radius caused a strong velocity gradient at the turbine inlet in the baseline, making it difficult to achieve a smooth blade loading from the hub to the shroud. However, this velocity distortion was decreased in the optimal geometry, hence attaining a smoother blade loading from the hub to the shroud. This is the reason why the optimal geometry produced the highest amount of output torque and, hence, the highest value of the power coefficient compared to the baseline. Therefore, it is

deduced that it is not only the inlet flow condition that is important for the turbine performance but also the inlet flow velocity distribution from the hub to the shroud. Moreover, from the findings, it was observed that horizontal tidal turbines with smaller hub radii and longer blades had better performance compared to those with a larger hub radius and smaller blades. This is because all the selected designs from the Pareto front had smaller hub radii and longer blades compared to the baseline.

From the internal flow analysis, the optimal geometry did not suffer any flow separation in the diffuser compared to the baseline. This is because swirl flow in the diffuser, due to the centrifugal force, suppressed the flow separation. This improved the pressure recovery in the optimal diffuser, resulting in higher C_{P0} values.

A sensitivity analysis was conducted to find out which design parameters had more influence on the performance of the turbine. The inflow velocity at the turbine inlet showed a good correlation with the power coefficient. The other parameters, including the diffuser length and hub radius, did not have a clear correlation with the power coefficient and were, therefore, deemed not important.

As a recommendation and future plan, experiments should be done to validate this model and the results. Blade loading improvement for the optimal design will also be confirmed experimentally.

REFERENCES

- [1] Y. Ohya and T. Karasudani, "A Shrouded Wind Turbine Generating High Output Power with Windlens Technology," *Energies*, 3, 634-649, 2010.
- [2] I. Hashem, M. H. Mohamed, and A. A. Hafiz, "Numerical Investigation of a Small-Scale Shrouded Wind Turbine with a Brimmed Diffuser," in *The Proceedings of 12th International Conference of Fluid Dynamics (ICFD12)*, Cairo, Egypt, 2016
- [3] S. Weichao, A. Mehmet, N. Rosemary, A. Batuhan and T. Serkan, "Numerical optimization and experimental validation for a tidal turbine blade with leading-edge tubercles," *Renewable Energy*, 96, 42-55, 2016.
- [4] Z. Fu-wei, D. Lan, H. Bin, B. Ming and L. Jin-Tao, "Blade design and optimization of a horizontal axis tidal turbine," *Ocean Engineering*, 195, 106652, 2020. https://doi.org/10.1016/j.oceaneng.2019.106652
- [5] D. Zhang, L. Ding, B. Huang, X. Chen, and J. Liu, "Optimization Study on the Blade Profiles of a Horizontal Axis Tidal Turbine Based on BEM-CFD Model," China Ocean Engineering, 33, 4, 436-445, 2019.
- [6] M. Kunasekaran, S.H. Rhee, N. Venkatesan, A. Samad, "Design Optimization of a Marine Current Turbine Having Winglet on Blade," *Ocean Engineering*, 239, (2021) 109877.
- [7] M. V. Smirnov, A. A. Sebelev, N. A. Zabelin and N. I. Kuklina, "Effects of Hub Endwall Geometry and Rotor Leading Edge Shape on Performance of Supersonic Axial Impulse Turbine. Part I," in *The Proceedings of the* 12th European Conference on Turbomachinery Fluid

- *Dynamics & Thermodynamics ETC* 12, Paper ID: ETC2017-100, Stockholm, Sweden, April, 2017.
- [8] M. B. Akin, P. Pieringer and W. Sanz, "Optimization of a Low Pressure Turbine Stage by Hub Endwall Contouring of the Turining Mid Turbine Frame Using an Adjoint Method," in *The Proceedings of the 12th International Symposium on Experimental Computational Aerothermodynamics of Internal Flows, ISAIF12-029*, Lerici, Italy, 2015
- [9] M. Fan, Z. Sun, R. Yu, X. Dong, Z. Li and Y. Bai, "Effect of Leading-edge Tubercles on the Hydrodynamic Characteristics and Wake Development of Tidal Turbines," *Journal of Fluids and Structures*, 119 (2023) 103873.
- [10] D. Zhang, D. Liu, X. Liu, H. Xu, Y. Wang, R. Bi and P. Qian, "Unsteady Effects of a Winglet on the Performance of a Horizontal-axis Tidal Turbine," Renewable Energy, 225 (2024) 120334
- [11] M. Khaled, M.M. Ibrahim, H.E.A. Hamed and A.F. AbdelGwad, "Investigation of a Small Horizontal-axis Wind Turbine Performance With and Without Winglet," *Energy*, 187 (2019) 115921.
- [12] B. Marina, B. Ivan and G. Zvonimir, "Numerical Study of the Flow Field around Hydrokinetic Turbines with Winglets on the Blades," *Renewable Energy*, 192 (2022) 692-704.
- [13] Y. Ren, B. Liu, T. Zhang and Q. Fang, "Design and Hydrodynamic Analysis of Horizontal Axis Tidal Stream Turbines with Winglets," *Ocean Engineering*, 144 (2017) 374-383.
- [14] Y. Ren, B. Liu and T. Zhang, "Influences of Winglets on the Hydrodynamic Performance of Horizontal Axis Current Turbines," Applied Ocean Research 92 (2019) 101931.
- [15] P. Savaranan, K.M. Parammasivam and S.S. Rajan, "Experimental Investigation on Small Horizontal Axis Wind Turbine Rotor Using Winglets," *Journal of Applied Science and Engineering*, Vol. 16, No. 2, pp. 159-164, 2013.
- [16] T. Nagataki, K. Kurokawa, D. Sakaguchi and Y. Kyozuka, "Optimization of a Horizontal Axis Tidal Current Turbine by Multiobjective Optimization," in The Proceedings of the ASME 2019 38th International Conference on Ocean, Offshore and Arctic Engineering, OMAE2019, Glasgow, Scotland, 2019
- [17] H. Sun, S. Yamaguchi and Y. Kyozuka, "Tidal Current Energy Assessment around Goto Islands, Japan, "in The Proceedings of The International Symposium on Marine and Offshore Renewable Energy (MORE), pp. 1-8, 2013.
- [18] D. Sakaguchi, and Y. Kyozuka, "Design of a Shrouded Tidal Current Turbine by Multi-Objective Optimization," in *Grand Renewable Energy* Conference, Yokohama, Japan, 2018.
- [19] M.T. Tun, D. Sakaguchi, R. Numakura and B. Wang, "Multi-Point Optimization of Recirculation Flow Type Casing Treatment in Centrifugal Compressors," in *The*

Proceedings of the ASME Turbo Expo 2016: Turbomachinery Technical Conference and Exposition, Seoul, South Korea, 2016. https://doi.org/10.1115/GT2016-56610

[20] D. Sakaguchi, M. Ishida, H. Hayami, L. Mueller, Z. Alsalihi and T. Verstraete, "Multipoint Multi-Objective Optimization of a Low Solidity Circular Cascade Diffuser in Centrifugal Blowers, "in The Proceedings of the ASME Turbo Expo 2014: Turbine Technical Conference and Exposition," Dusseldorf, Germany, 2014. https://doi.org/10.1115/GT2014-26013

APPENDIX

I. Design parameters for optimization of the Water Lens Turbine as summarized in Table 1.

Opt-1 is the blade angle, β_1 at the leading edge (LE) at the hub side.

Opt-2 is the difference between β_2 and β_1 at the hub side. Whereby β_2 is the blade angle at a control point along the chord between the LE and the trailing edge (TE) of the blade.

Opt-3 is the difference between β_3 and β_2 at the hub side.

Whereby β_3 is the blade angle at the blade TE.

Opt-4 is the meridional position of the blade TE with reference from the LE at the hub side.

Opt-5 is the nacelle cylinder radius

Opt-6 is the hub taper radius

Opt-7 is the span position of control points (Opt-8 and Opt-9)

Opt-8 is the blade angle at the LE

Opt-9 is the blade angle at the TE

Opt-10 is the blade angle, β_1 at the leading edge (LE) at the shroud side.

Opt-11 is the difference between β_2 and β_1 at the shroud side. Whereby β_2 is the blade angle at a control point along the chord between the LE and the trailing edge (TE) of the blade

Opt-12 is the difference between β_3 and β_2 at the shroud side. Whereby β_3 is the blade angle at the blade TE.

Opt-13 is the meridional position of the blade TE with reference from the LE at the shroud side.

Opt-14 is the shroud inlet length

Opt-15 is the shroud inlet radius

Opt-16 is the shroud outlet length 1

Opt-17 is the shroud outlet radius 1

Opt-18 is the shroud outlet radius 2